Pharm Res (2013) 30:269–279
DOI 10.1007/s11095-012-0871-9

RESEARCH PAPER

Metal Ions Guided Self-assembly of Therapeutic Proteins for Controllable Release: From Random to Ordered Aggregation

Kai Shi • Fude Cui • Hongshu Bi • Yanbo Jiang • Hang Shi • Tao Song

Received: 23 May 2012 / Accepted: 20 August 2012 / Published online: 14 September 2012

ABSTRACT

Purpose To make a comparative study on sustained delivery performance of rhIFN with random amorphous and spherical crystal-like ordered self-assemblies.

Methods The rhIFN self-assemblies were identified in batch crystallization mode. Physico-chemical characteristics were compared, including morphology, XRD, FTIR, CD, biological potency, the dissolution behaviors *in vitro* and plasma pharmacokinetics *in vivo*. Moreover, molecular simulation was performed to better understand their binding site and mode.

Results Here, we suggest that random amorphous and spherical ordered self-assemblies allow for long action without new molecular entities generation or carriers employed. By manipulating supersaturation, the ordered aggregates were self-organized at high concentration of Zn(II) (>100 mM) in pH 5.5–6.0, which was the first time that spherical semi-crystals of rhIFN can act as a depot source for the sustained delivery of biologically active proteins. The secondary structure and biological potency of rhIFN were unchanged after aggregation. Compared with that of the native rhIFN, both self-assemblies exhibited slower absorption and extended elimination profiles after s.c. administration, which were characterized as 4.75 ± 0.82 h and 10.58 ± 1.86 h of terminal half-life for random amorphous and spherical ordered self-assemblies, respectively.

Conclusions The work described here demonstrates the possibility of self-assemblies of biomacromolecules for controllable release application of therapeutic proteins.

KEY WORDS controllable release · interferon · protein delivery · self-assembly · spherical crystal

INTRODUCTION

With the great progress in the field of recombinant biotechnology, numerous protein based drug candidates have been produced in commercial quantities and evaluated for therapy of various pathologic conditions such as diabetes mellitus, endocrine disorders, autoimmune disorders and specific metabolic abnormalities (1,2). Despite of the promising pharmacological activities, the dosing of these therapeutic proteins is often limited to the frequent parenteral injection currently due to their low stability and thus rapid clearance *in vivo* (3). For example, recombinant human interferon (rhIFN) alpha, a kind of cytokines with broad spectrum antiviral and antiproliferative effects in the treatment of cancer and virus related diseases, has a short serum half-live of 2–6 h and characteristically shows a "burst" or a "pulse" profile in blood levels when injected subcutaneously (4). Thus frequent administration of doses of the protein must be made to maintain a therapeutically effective blood serum concentration of the drug, which usually results in patient incompliance and serious side effects occurrence such as fever, headache, nausea, diarrhea mild anxiety and even depression (5,6).

Therefore there are clinical situations where a need to design a novel formulation in which the protein is

K. Shi (✉) · F. Cui · Y. Jiang · H. Shi
Department of Pharmaceutics, School of Pharmaceutical Science
Shenyang Pharmaceutical University
No. 103, Wenhua Road
Shenyang 110016, China
e-mail: kaishi_syphu@hotmail.com

H. Bi
Liaoning Yilian Institute of Materia Medica
No. 18, Sanhao Street
Shenyang 110004, China

T. Song
Liaoning Satellite Biotechnology Products Research Institute
No. 51-3, Dongzhan Street
Shenyang 110044, China

continuously released into the blood stream so that the serum drug concentration reaches a plateau and remains at that level for a period of time. Among the possible strategies to achieve the goal, such as biodegradable polymer depots (7,8), liposome (9), hydrogel (10) and polyethylene glycol (PEG) covalent conjugates (11), pure protein self-assemblies in random or ordered aggregates provide us a promising alternative. In comparison with small drug molecules, proteins generally will tend to form self-assemblies with reduced solubility under a variety of environmental conditions, such as pH, ionic strength, temperature, salt type and concentration (12). So it can act as a source for the release of proteins due to the solubility-limiting dissolution process. Depending on progress supersaturation employed, the self-assemblies generally present variable forms. Some self-assemblies display an random organization in amorphous shape, whereas others form highly ordered crystal-like organizations, suggesting that protein self-assemblies may be a common structural property of polypeptide chains (13). Although some changes in structure conformation and thus reduced bioactivity are often encountered due to the irreversible aggregation, these desirable characteristics will be fortunately avoided through reversible protein self-assemblies mediated with metal ions chelation (14).

Metal ions often play a critical role in maintaining the correct conformations for many proteins. An excessive amount of zinc is needed to maintain hexameric insulin in a stable state (15). Both Cu(II) and Zn(II) are indispensable metal ligands for reduction activity of superoxide dismutase (SOD) (16). Moreover, metal ions can facilitate reversible aggregation of proteins while have less effects on their biological potency. This process is generally mediated through effects of metal ions chelation (17). It is known that proteins, specifically those containing histidine, cysteine, methionine, glutamic acid, aspartic acid, lysine, and tyrosine, have strong electron donor groups in their side chains (like imidazole ring, sulfhydryl group and carboxylic group) and can act as Lewis base to complex with metal ions, especially some divalent ions such as Zn(II), Co(II), Ca(II) and Mg(II). The complex formation will lead to a higher supersaturation and promote formation of protein self-assemblies.

Therefore in the self-assembly aggregates of therapeutic proteins, whether random or ordered forms, the proteins exist as a binding manner and held together by some intermolecular forces, such as the hydrophobic interactions, H-bonds, salt bridges, *etc.* (18). Compared with their native forms, the protein self-assemblies can protect the physical-chemical and biology integrity in the aggregated structures during processing, upon storage and after drug release (19,20). Depending on the different affinities between molecules, the protein self-assemblies may possess varied dissolution characteristics, which make the possibility of controllable release of the therapeutic agents for an effective duration without any other carrier materials used. Thus the safety issues that are raised by the common capsulation vehicles from synthetic or native materials should not be presented by the pure protein self-assembly based depots. Moreover, the simplicity and mild conditions required to form the protein self-assemblies, means the potential labor and cost advantages over conventional formulations (21).

Hence, the main aim of this work was to make a comparison research on the controllable release performance of various rhIFN self-assemblies, including random and ordered crystal-like aggregates. The structure characterization of the self-assembly aggregates, including morphology, X-ray diffraction, Fourier transform infrared spectrum (FTIR), circular dichroism (CD) and biological potency evaluations were studied. To explore the possibility of manipulating the release rate of the developed formulation, the *in vitro* dissolution behavior and *in vivo* serum pharmacokinetics of subcutaneous administration of various self-assembly aggregates were also investigated. Moreover, molecular kinetics simulation was carried out to better understand the process mechanism of metal ions guided self-assembly and thus the modified release behaviors.

MATERIALS AND METHODS

Materials

Recombinant human interferon-α-2b (rhIFN), with a non-glycosylated polypeptide chain containing 165 amino acid residues (19.3 kDa) and biological potency of 1.36×10^8IU/mg, was expressed in Escherichia coli and provided by Huaxin High Biotechnology Inc. (Shanghai, China). Human interferon alpha enzyme-linked immunoassay (ELISA) kits were supplied by Lichen Biological Science and Technology Co., Ltd. (Shanghai, China). All other reagents and chemicals were of analytical grade.

Screening of Random and Ordered Self-assemblies of rhIFN

The conditions with various rhIFN self-assemblies obtained were identified and successfully scaled up by batch crystallization mode. Briefly, protein solution containing 40 mg/mL rhIFN in 0.5 M acetate buffer was mixed with concentrated crystallization solution containing zinc acetate to achieve the final concentrations of 50 ~ 200 mM zinc ions and pH 5 ~ 7. The resulting solution was incubated at 4°C for 48 h until various self-assembly aggregates of rhIFN occurrence. The obtained rhIFN-Zn(II) chelate self-assemblies were isolated from mother liquor and washed two times with distilled water to remove unbound zinc ions. Then freeze drying of the resultant self-assemblies were carried out for subsequent physical characterization.

Physical Characterization

The surface morphology and detail structure of rhIFN self-assemblies were examined with scanning electron microscopy (SEM) analysis. All samples were mounted on aluminum stubs, followed by gold metallization using an ion sputter coater (Hitachi E101, Tokyo, Japan) and observed on a Hitachi S-2400 N scanning electron microscope (Tokyo, Japan). Observations of rhIFN self-assemblies in suspension were also made using light microscope (Motic DM-BA400-B, China).

X-ray diffractograms (XRD) were determined using a PANalytical X'Pert Pro diffractometer equipped with a PIXcel detector (PANalytical B.V., Almelo, Netherlands). Samples were placed on zero-background silicon plates and measured at ambient conditions in reflection mode. A continuous 2θ scan was performed with the diffraction angle increasing from 5° to 40°, with a step size of 0.026° using Cu K_α radiation. The voltage and current applied were set as 30 mA and 30 kV, respectively. Data were collected using X'Pert Data Collector software and processed using X'Pert HighScore Plus (PANalytical B.V.). The XRD patterns of self-assemblies were verified, comparing to that of bulk drug and zinc acetate.

Fourier transform infrared spectroscopy (FTIR) was used to characterize the complex formation of rhIFN self-assemblies. The rhIFN-Zn(II) chelate self-assemblies in powder form was tested using a FTIR Spectrometer (BRUKER IFS-55, Switzerland). The infrared spectra of native rhIFN, zinc acetate and their chelate self-assemblies were obtained by the KBr method.

Circular dichroism spectra (CD) were utilized to illustrate the changes in secondary structure of rhIFN in self-assemblies. The rhIFN-Zn(II) chelate self-assemblies were dissolved in PBS (0.1 M, pH 7.4) and scanned from 250 to 200 nm at a scanning speed of 5 nm/min for far-UV CD analysis. All CD measurements were conducted with a CD spectropolarimeter (Bio-Logic MOS 450, France, Grenoble) equipped with a temperature control device. The generated ellipticity values were subsequently converted to molar ellipticities using the equation $[\theta]_\lambda = \theta_\lambda / C \cdot L$, where θ_λ is the observed ellipticity at the wavelength λ, C is the decimolar rhIFN concentration and the L is the pathlength in the decimeters.

The Zn(II) bound with rhIFN in self-assemblies were determined by a modified 1-(2-Pyridylazo)-2-naphthol (PAN) colorimetric method. Briefly, approximate 3 mg washed rhIFN-Zn(II) chelate aggregates were added into 4 ml ammonia buffer (0.5 M, pH 10) containing 10% (w/w) Triton X-100 and 0.05% (*w/v*) PAN. The absorbance of resultant solution was measured at the wavelength of 525 nm for zinc ions analysis.

Cytopathic Effect Inhibition Assay

To determine the biological potency retention of rhIFN in self-assemblies, a cytopathic effect inhibition assay was performed. The vesicular stomatitis virus (VSV) was used to produce cytopathic effect on the human amnion WISH cells. In briefly, WISH cells (3.5×10^5 cells/ml) were seeded in a 96-well microtiter and incubated with 4-fold serial dilutions of rhIFN samples for 24 h at 37°C. After the virus diluent (100 $CCID_{50}$) was added, the plates were incubated for 24 h until the cytopathic effect with 90% cell lysis was evident in the virus control wells. WISH cell viability was determined by measuring the absorbance of crystal violet-stained living cells in an ELISA plate. The relative potency of rhIFN was expressed as percentage of dilution multiples difference that shows 50% protection of VSV-induced WISH cells (ED_{50}) between the self-assembly and standard rhIFN samples.

Dissolution Kinetics Studies *In Vitro*

In vitro rhIFN dissolution from self-assemblies was performed in artificial extracellular fluid (Dulbecco's phosphate-buffered saline, without $CaCl_2$ and $MgCl_2$, pH 7.4) at 37°C with continuous orbital mixing (50 r/min). At appropriate intervals, the entire suspensions were subjected to centrifugation at 5000 g for 5 min. The resulted pellets were re-suspended in equal volume of fresh dissolution medium. The amount of rhIFN dissolved in the supernatant was evaluated by size-exclusion liquid chromatography (SEC-HPLC) analysis. The chromatographic system (Shimadzu, Japan) consisted of a LC-10AT pump, a SPD-M10A VP UV–vis detector, a CTO-10AS VP column oven and a CLASS-VP Workstation. Chromatographic separation was performed on a Protein-Pak 125 column (300 × 7.8 mm ID, Waters, USA). The column was eluted with phosphate-buffered saline at the flow rate of 1.0 ml/min, and eluent was monitored at 214 nm. The cumulative rhIFN percentage dissolved from the self-assemblies was calculated as the ratio of the amount of rhIFN dissolved at time (t) to the initial amount used.

Pharmacokinetics and Statistical Analysis

Healthy rabbits that weighed 2.0 ± 0.1 kg were used and fasted overnight prior to the experiments. The animals were randomly assigned into three groups (five rabbits per group) followed by administration of soluble, random and ordered rhIFN self-assemblies by subcutaneous injection at a single dose of 7.5×10^6 IU/kg, respectively. The self-assembly aggregates were suspended in aqueous solution consisting sodium carboxy methyl cellulose (0.5% *w/v*) and mannitol (5.0% *w/v*) before subcutaneous injection. Blood samples

were collected at determined time intervals followed by coagulation and centrifugation at 5000 g for 5 min. The resulting serum layers were separated and stored at −80°C until ELISA analysis. All procedures were conducted in accordance with the Animal Ethical Guidelines for Investigations in Laboratory Animals and were approved by the Ethical Committee for Animal Experimentation of the Shenyang Pharmaceutical University.

The mean serum concentration profiles for each rhIFN formulation were constructed. The pharmacokinetics parameters of terminal half-life ($t_{1/2}$), mean residence time (MRT), the area under the concentration–time curve (AUC) from $t=0$ to last sampling time (AUC_{last}) and extrapolated time (AUC_{total}) were derived from the profiles using a non-compartmental model of WinNonlin® software package (Pharsight Corporation, USA). The relative bioavailability (F) was calculated based on the following equation:

$$F = \frac{AUC_{aggre.}}{AUC_{sol.}} \times \frac{Dose_{sol.}}{Dose_{aggre.}} \times 100\% \quad (1)$$

The experimental data are expressed as mean ± standard deviation. Statistical significance was assessed using a standard unpaired Student's *t*-test with $p<0.05$ being considered significant.

Molecular Simulation

The binding modes of Zn(II) to rhIFN were explored using molecular simulation. The protein coordinates were extracted from the Protein Data Bank (www.pdb.org) with PDB ID: 1RH2 for rhIFN alpha-2b. The simulation results were viewed in Molsoft ICM-Pro® (Molsoft L.L.C., USA). The van der Waals, hydrogen bonds, desolvation and torsional parameters were those implemented by default in the software.

RESULTS

Formation of rhIFN Self- assembly Aggregates

To specify the conditions for formation of random and ordered self-assemblies respectively, 3D contour diagrams showing the effects of Zn(II) concentration and solution pH on aggregates yields were first constructed according to the results of screening experiments. As illustrated in Fig. 1, the supersaturation degree needed for random and crystal forms are varied. At low concentrations of Zn(II) (<20 mM) and pH (<5.0), the solution remains clear and without any protein aggregation appearance at any time. The high concentrations of Zn(II) (>200 mM) and pH (>7.0) always result in an amorphous precipitation occurrence (seen in Fig. 1a). It can be found that pH, rather than Zn(II) concentration, played an important role in the type of varied aggregates. In the range of high concentration of Zn (II) (>100 mM), the area for ordered crystals formation only can be available in pH 5.5–6.0 at 48 h after seeding, higher pH always leaded to amorphous precipitates formation immediately. Moreover, both aggregates are performed at 4° C, higher temperature would result in lower supersaturation degree and none aggregates available.

Characterization of rhIFN Self-assembly Aggregates

Different from normally ordered crystals with regular geometric shape, it can be found in optical microscopies that the crystal-like self-assemblies were formed in spherical aggregates and characterized as rough surface and particle diameter in about 18–30 μm (Fig. 2a). In contrast with that of ordered aggregates, precipitate-like aggregates showed very smaller size (<1 μm) and amorphous in shape (Fig. 2b).

In view of somewhat indirect for optical evidence that is limited by low depth of field and insufficient resolution to

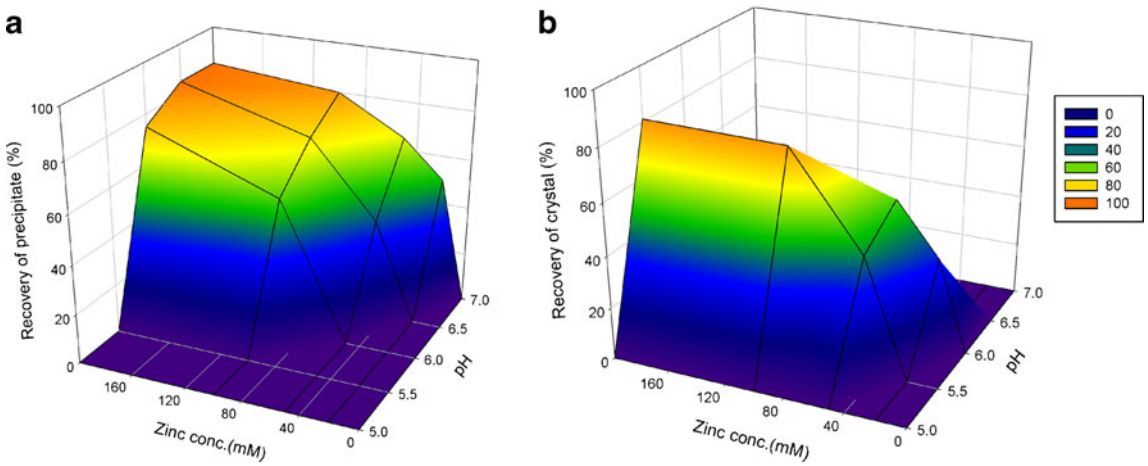

Fig. 1 3D contour plots for effects of Zn(II) concentration and pH on the recovery of rhIFN random amorphous (**a**) and ordered self-assemblies (**b**). The spectrum colors represent yields percent of aggregates.

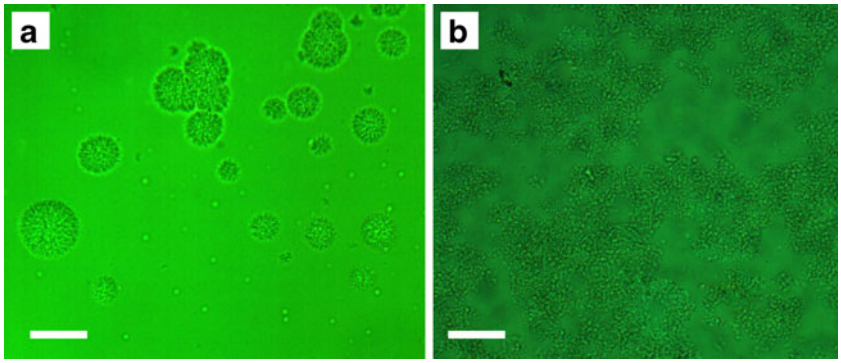

Fig. 2 Typical optical microscopic images of rhIFN self-assemblies in spherical crystal-like ordered form (**a**) and random amorphous form (**b**). Scale bar in all pictures, 20 μm.

see more fine morphology, scanning electron microscope (SEM) was performed to try to clarify the intrinsic structure of the aggregates. As shown in Fig. 3a, the crystal-like ordered self-assemblies of rhIFN were characterized as monodisperse spherical in shape. The outer surface of crystals looks rough and filled with hollow cells formed between thin vertical lamellaes, which makes them a "honeycomb" like structure (Fig. 3d). As seen in Fig. 3c, it seems that the spherical crystal-like ordered self-assemblies were formed by nucleation from an amorphous core, and growth into the micrometer range as radically oriented branching lamellaes by the addition of rhIFN molecules from solution. Compared with that of spherical crystal-like ordered self-assemblies, the random aggregates were in amorphous shape with a diameter of about 0.3–0.5 μm (seen in Fig. 3b).

The structures of rhIFN- Zn(II) chelate self-assemblies were studied by FTIR spectroscopy to examine whether the native structure of the protein was retained in the aggregates. The infrared spectra of zinc acetate, native rhIFN, and their chelate random and ordered self-assemblies are shown in Fig. 4. It's known that the amide I band of proteins in FTIR spectra (1600 and 1700 cm^{-1}) has been widely used as an indication for the secondary structure conformation of protein (22). As shown in Fig. 4, amide I bands of the rhIFN in the random and ordered self-assemblies were similar to that of native one, suggesting that the secondary structure conformation of rhIFN in the aggregates were unchanged. However, there was a difference between the native and the Zn(II) chelate self-assemblies in their FTIR spectra, which is corresponding to the significant changes in intensity but little in displacement of characteristic absorption peaks in the chelate self-assemblies. In addition, no new peaks were observed in the both random and ordered self-assemblies. These observations suggest that some weak physical interactions between rhIFN and Zn(II) take place during the metal ions chelation guided protein self-assembly.

Figure 5 shows the powder X-ray diffraction patterns of zinc acetate, native rhIFN, random and ordered self-assemblies of rhIFN. The diffraction patterns of both native rhIFN and random aggregates shown in Fig. 5c, d are amorphous lacking crystalline peaks. Whereas for spherical

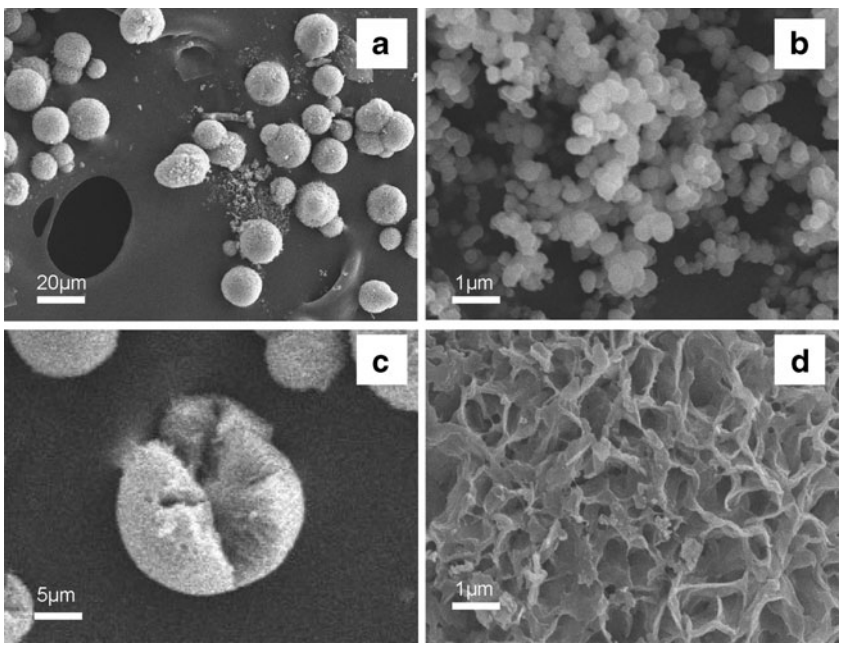

Fig. 3 SEM morphology of rhIFN self-assemblies. (**a**) Overall appearance of rhIFN spherical crystal-like ordered form. (**b**) Overall appearance of rhIFN random morphous form. (**c**) Local close-up features of inner structures for rhIFN spherical semi-crystals, in where nucleation site were found in the core of ones with growth defects. (**d**) Local close-up features of surface morphology for rhIFN spherical semi-crystals.

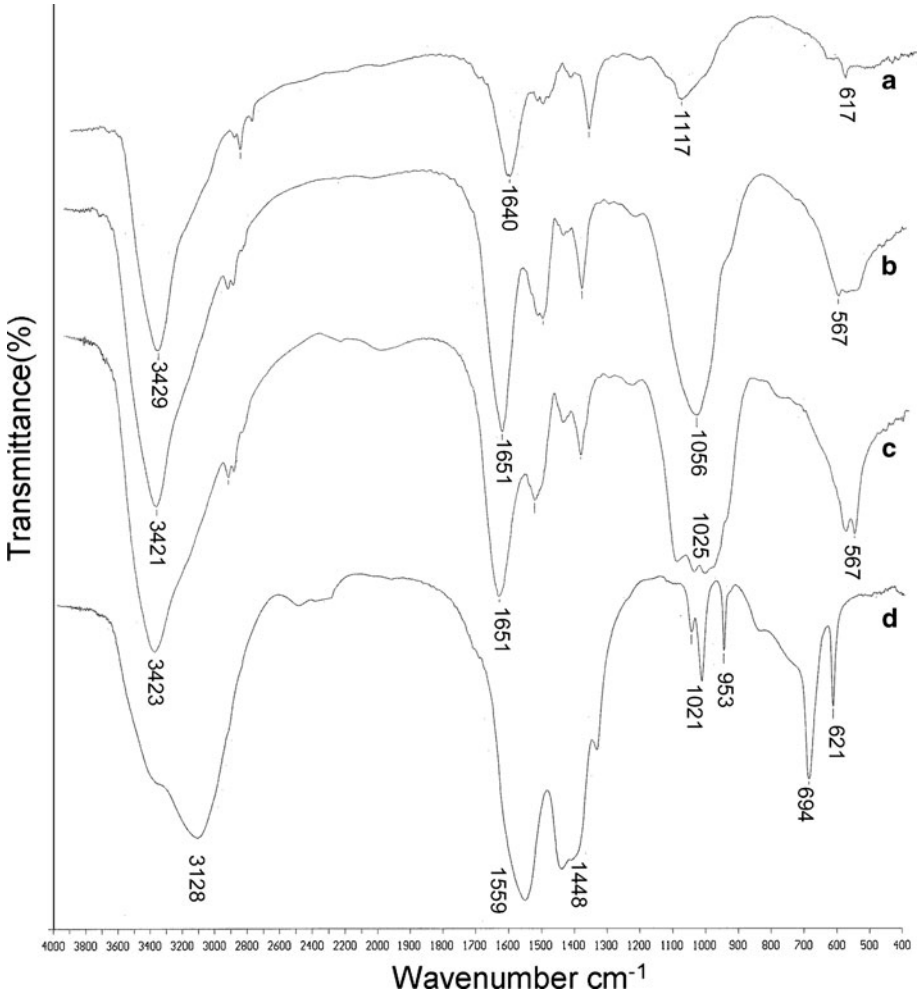

Fig. 4 Infrared spectra of native rhIFN (**a**), random amorphous self-assemblies (**b**), spherical crystal-like ordered self-assemblies (**c**) and zinc acetate (**d**).

ordered self-assemblies, there are several detectable sharp crystalline peaks observed in the range of 20° to 35° apparently, suggesting that the spherical ordered self-assemblies have possessed partial crystallinity (Fig. 5b). It can be also observed that the sits of crystalline peaks in zinc acetate are different completely from that of spherical ordered self-assemblies (seen in Fig. 5a).

To further assess the secondary structure conformation of the rhIFN in the aggregates, a far-UV CD spectrum of the self-assemblies in an aqueous medium was measured and compared with that of the native rhIFN solution (seen in Fig. 6). The shape of the CD spectra is typical of α-helix and does not indicate a considerable presence of ß structure. It can be found that in the far-UV region, there are two major negative maximal bands at 222 nm and 208 nm resulted from Cotton effects of α- helix, where the first extremum corresponds to the n-π* transition of the peptide bond, and the second is due to the π-π* transition (23). Both extrema yield similar information of the conformation of the protein, however, only the data from the 222 nm region were evaluated for calculating α-helical content of the rh-IFN in various self-assemblies because of a better signal-to-noise ratio. As shown in Table I, Analysis of the spectrum of rhIFN in random and spherical ordered self-assemblies yielded an estimate of the α-helical content of approximately 47.9% and 49.3%, respectively. Both contents are little

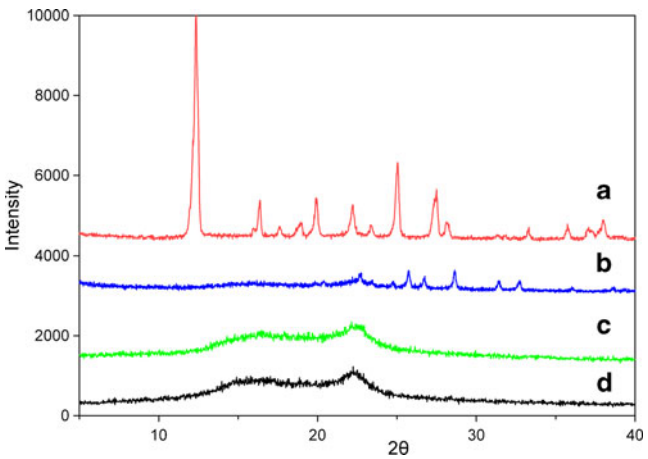

Fig. 5 X-ray diffraction patterns of zinc acetate (**a**), spherical crystal-like ordered self-assemblies (**b**), random amorphous self-assemblies (**c**) and native rhIFN (**d**).

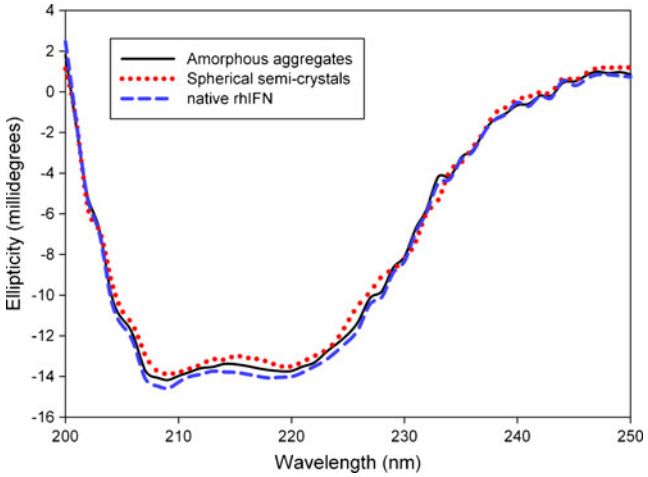

Fig. 6 Far-UV CD spectrum of spherical crystal-like ordered self-assemblies (…), random amorphous self-assemblies (—) and native rhIFN (– – -).

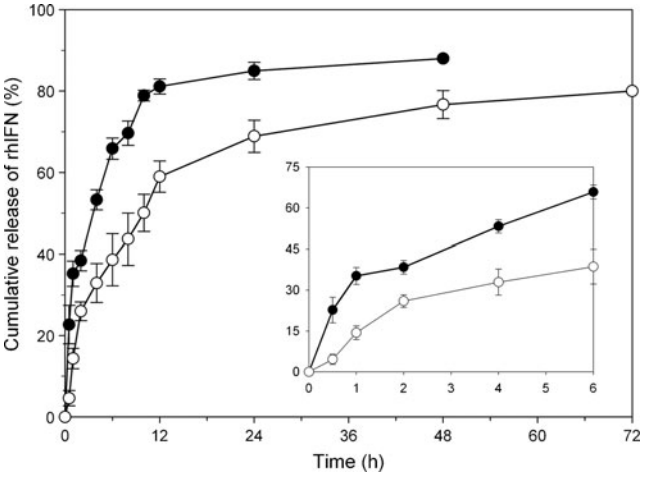

Fig. 7 *In vitro* dissolution profiles of rhIFN from spherical crystal-like ordered self-assemblies (*Black circle*) and random amorphous self-assemblies (*White circle*). The inserted panel depicts the difference in initial burst release behaviors of different self-assemblies within the first 6 h. All data are represented as means ± SD (n=3).

lower than that of native rhIFN (52.8%) while the difference is not statically significant ($P>0.05$), indicating that the secondary structure conformation of rhIFN was not perturbed in the self-assemblies.

In order to determine the molar ratio of chelate Zn (II) to rhIFN in the self-assemblies, a modified PAN colorimetric method was employed for zinc ions analysis, which has been used for the spectrophotometric trace analysis of numerous metal ions (24). As for zinc and PAN, an orange-colored metal chelate can be formed between them, which is almost insoluble in water and the analysis is generally assisted by solubilization of the metal chelates with nonionic surfactant. The solubilized zinc chelate showed a maximum absorption at 525 nm and was constant at the pH range from 9.2 to 10.2. The analysis gave a 2.7±0.4 molar ratio of zinc to rhIFN for ordered self-assemblies and 2.1±0.3 molar ratio of zinc to rhIFN for amorphous random self-assemblies.

In Vitro Release and Bioactivity Assay of rhIFN Self-assembly Aggregates

In vitro dissolution profiles of rhIFN from various self-assemblies were investigated in artificial tissue fluid (pH7.4) at 37°C. As shown in Fig. 7, there is a strong dependence of the dissolution rates on the aggregate forms. For these formulations, a higher ordered self-assembly to rhIFN resulted in a lower initial burst and release rate. The spherical ordered self-assemblies yielded an initial burst of 14.3% in the first 1 h as comparable to 35.2% for amorphous ones. It was also found that in the form of amorphous random self-assemblies, near 80% of protein was released over 12 h. Changing aggregate form into ordered self-assemblies did help to improve the *in vitro* dissolution characteristics of rhIFN, which was indicated by 72 h for the overall release period of protein loaded.

The corresponding changes in biological potency retention of rhIFN from various self-assemblies during *in vitro* release are shown in Fig. 8. An obvious lost in cytopathic effect inhibition of native rhIFN can be found with only 60% remained over the release period. However, there were still significant levels of rhIFN bioactivity remained in aggregates for 72 h when incubation at 37°C, whether for random or ordered self-assemblies. Compared with that of random ones, the spherical ordered self-assemblies possess more stability due to their ordered structures as revealed in SEM analyses.

In Vivo Pharmacokinetics Studies of rhIFN Self-assembly Aggregates

To compare the ability of various self-assemblies to produce sustained blood drug levels, the pharmacokinetic behaviors of random and ordered self-assemblies were evaluated in health rabbits *via* subcutaneous administration at a single dose of 7.5×10^6IU/kg, respectively. The

Table I Mean Secondary Structure Composition (%) of rhIFN in Self-Assemblies. (n=3)

Sample	Alpha helix	Beta sheet	Beta turn	Random-coil
Native rhIFN	52.8±1.5	7.4±0.9	11.7±1.0	28.0±1.1
Random self-assembly	47.9±1.9	9.6±0.8	15.5±2.1	26.9±0.8
Ordered self-assembly	49.3±2.3	10.6±1.0	12.8±1.3	27.2±1.4

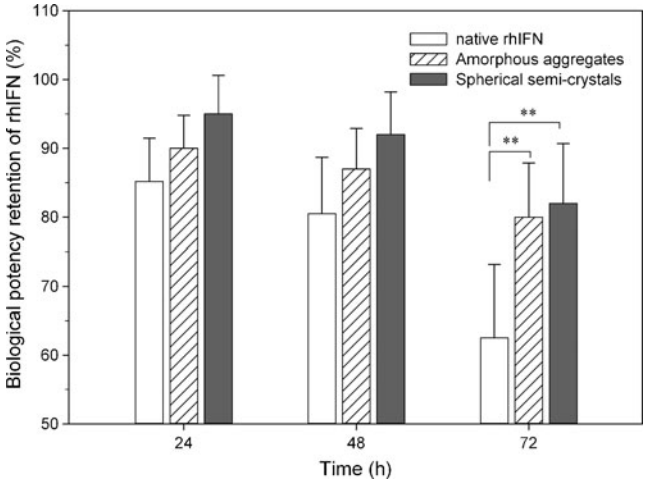

Fig. 8 The bioactivity retention of rhIFN in native rhIFN, spherical crystal-like ordered and random amorphous self-assemblies during *in vitro* release period. Statistically significant difference from native rhIFN. (*$p < 0.05$, **$p < 0.001$).

native rhIFN solution in Tris buffer (10 mM, pH 7.4) with the same single dose was set as control group. The changes in level of serum rhIFN concentrations *versus* time *in vivo* for various self-assemblies are shown in Fig. 9. The phamacokinetic parameters were determined from the serum drug concentration-time data and analyzed using a noncompartimental pharmacokinetic model. The calculated parameters, including C_{max}, T_{max}, $t_{1/2}$, MRT and AUC are shown in Table II.

As seen in Table II and Fig. 9, subcutaneous administration of soluble rhIFN solution in rabbits resulted in a sharp increase in serum rhIFN concentration with a higher C_{max} value of 1411.10±575.28 IU/mL that were reached at approximately 2 h post-dosing. The followed rapid decline in the next 8~10 h led to 1.35±0.35 h of terminal half-life ($t_{1/2}$) and 3.88±1.02 h of mean residence time (MRT) respectively, indicating a rapid absorption and elimination behavior without ability of tailoring the pharmacokinetic profiles for common soluble native rhIFN solution.

Compared with that of the soluble native rhIFN, all of rhIFN self-assemblies exhibited slower absorption and extended elimination profiles at different degree, depending on the self-assembly forms of rhIFN. The Zn(II) chelate amorphous self-assemblies showed a significantly lower C_{max} of 823.60±357.28 IU/mL at about 6 h post-dose. The corresponding terminal $t_{1/2}$ and MRT were also extended to 4.75±0.82 h and 9.52±2.16 h, respectively. The serum rhIFN concentration above the lower limit of quantitation (8 IU/mL) can be observed for 24 h after dosing, which has double fold increase compared with that of soluble native rhIFN and suggests an improved ability for tailoring the pharmacokinetic profiles. In addition, despite their slower absorption behaviors, the amorphous aggregated rhIFN showed a bioavailability of (99.62±11.89)% relative to soluble native forms, indicating an almost complete absorption when exposure *in vivo*.

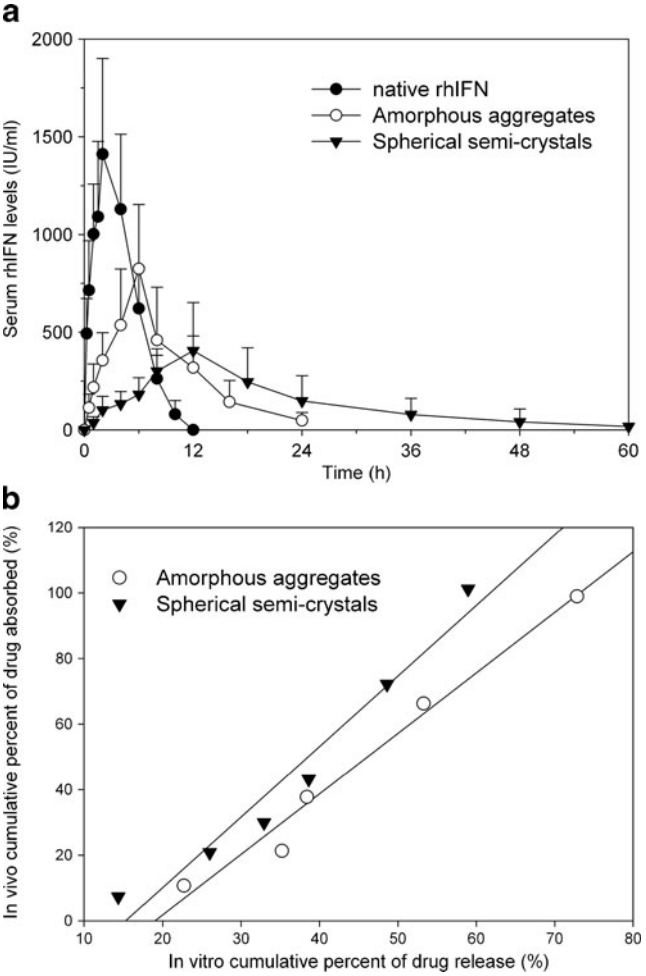

Fig. 9 (**a**) The serum rhIFN levels after s.c. administration of rhIFN (*Black circle*), spherical crystal-like ordered self-assemblies (*Black down-pointing triagle*) and random amorphous self-assemblies (*White circle*). Data represents the mean ± SD., n=5 per group. (**b**) IVIVC correlation between the *in vitro* release of rhIFN from self-assemblies (spherical crystal-like ordered and random amorphous forms) and the rhIFN plasma concentration in rabbits.

It can be found in Fig. 9 that s.c. administration of spherical ordered self-assemblies of rhIFN resulted in more significant prolonged duration time of rhIFN blood levels up to 60 h, which were characterized as the terminal $t_{1/2}$ and MRT extending to 10.58±1.86 h and 21.10±3.31 h, respectively. Accordingly, the C_{max} was decline to 385.26±143.19 IU/mL^{-1} at retard T_{max} of about 12 h post-dose. The relative bioavailability (F%) of spherical ordered self-assemblies of rhIFN after s.c. administration at the dose of 7.5×10^6IU/kg were estimated as (104.91±19.6)%, which is little more than that of amorphous one while the difference is not statically significant (P>0.05).

Table II Pharmacokinetic Parameters for Serum rhIFN Levels in Rabbits after s.c. Administration of rhIFN in Self-Assemblies ($n=5$)

Parameter	Native rhIFN	Random self-assembly	Ordered self-assembly
AUC_{last} ($IU \cdot h \cdot mL^{-1}$)	7198.36 ±1864.61	6998.25 ± 1938.41	7646.4 ± 1152.60
AUC_{tot} ($IU \cdot h \cdot mL^{-1}$)	7354.23 ± 1239.50	7326.64 ± 1304.36	7715.1 ± 1415.35
MRT (h)	3.88 ± 1.02	9.52 ± 2.16	21.10 ± 3.31
$t_{1/2}$ (h)	1.35 ± 0.35	4.75 ± 0.82	10.58 ± 1.86
C_{max} (h)	1411.10 ± 575.28	823.60 ± 357.28	385.26 ± 143.19
T_{max} (h)	1.80 ± 0.45	6.00 ± 1.40	13.20 ± 2.68
F (%)	NA	99.62 ± 11.89	104.91 ± 19.6

DISCUSSION

This work investigates the potential of using two kinds of protein self-assemblies in amorphous random and spherical ordered forms for local sustained release application. The concept of using protein amorphous aggregates with the aid of metal ions chelation has been issued for some time, which led to a decrease in solubility of the protein (19,25). Although tailored release was achieved, they do not have sufficient acting duration to meet the clinical needs. So spherical crystal-like ordered self-assembly, a special kind of protein aggregates in semicrystalline form, were employed in this work to adjust the release profile through co-crystallization with Zn(II). Like small chemical molecule ones, protein crystals are solids with ordered packing of the molecular units into defined lattice space groups. In the crystal-like organization, the proteins exist as a highly ordered manner and held together by some intermolecular forces, such as the hydrophobic interactions, H-bonds, salt bridges, *etc.*(26). So compared with their native or random amorphous forms, the crystallized therapeutic proteins can protect the physical-chemical and biology integrity in the lattice structure during processing, upon storage and after drug release.

Spherical crystal-like ordered self-assemblies of proteins are most commonly characterized as semicrystalline structure, which nucleate on a core and grow by the addition of precursor protein units from the solution to lamellae plates ends on the surface (27). As shown in possible schematic structure model of the self-assemblies (seen in Fig. 10), with the spherical self-assemblies expanding, the gaps between the growing lamellas from regular arrangement of polymer chains would be filled by the lamellas branching and random coiling polymers to produce a three-dimensional structure. In absence of thermal gradient, growth occurs radially in all directions resulting in spherical aggregates. This structure is different from either lamellar spherulites of synthetic polymers (such as polyethylene) or amyloid fibril spherulites of denatured proteins (such as insulin) previously reported (28,29).

Like crystallization of small molecules, spherical ordered self-assembly of biomacromolecules also follows most general theories on nucleation and crystal growth, in which the driving force for crystallization is the difference between the solubility and supersaturation of the protein (30). Supersaturation is a function of the concentration of the macromolecule and environmental parameters that affect its solubility.

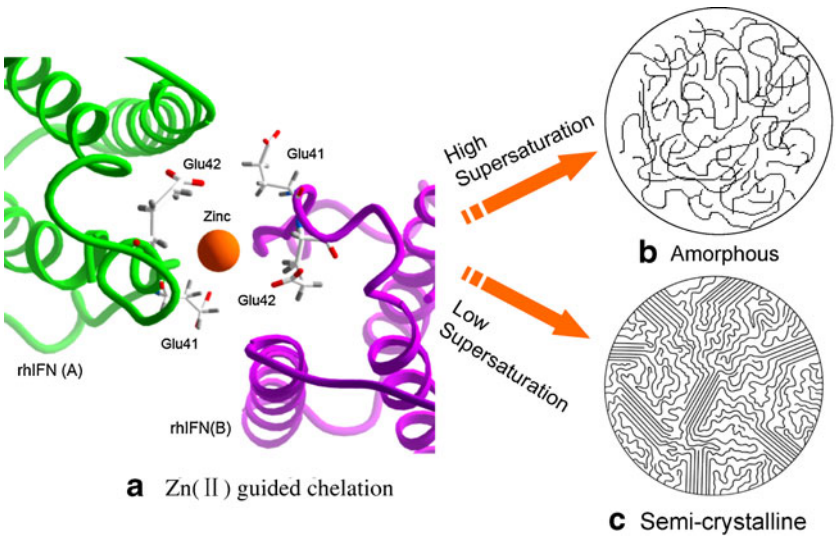

Fig. 10 Molecular models for the interaction of rhIFN with zinc ion (**a**). This view represents a look down the z-axis of the two interacting molecules. The α-helical sections of rhIFN are shown in violet and green ribbons and zinc ion in orange sphere. The chelation complex result in a decrease in solubility of the protein and thus formation of random amorphous (**b**) and spherical crystal-like ordered self-assemblies (**c**) according to the supersaturation employed.

It is achieved at high macromolecular concentrations, and at increasing values of precipitants that decrease macromolecular solubility. The protein solubility, depending on the surface charge of macromolecule, can be influenced by many factors which are usually quite sensitive to environment, like pH and temperature (31). It's well known that the optimal pH target for crystallization of a protein should be its isoelectric point, pI. This was intuitively appealing because at its pI, a macromolecule carries an equal number of positive and negative charges and is therefore electrostatically neutral. In all screening procedures, the pH values of protein solution were kept within the range of 5.5–6.0 which is equal to pI of rhIFN (32). This would seem to be the best situation for mutually attractive electrostatic interactions and thus a greater likelihood of rhIFN spherical ordered self-assembly to occur.

Besides achieving desired release profiles, the main challenge of protein and peptides delivery is to maintain the bioactivity of the biomacromolecules during and after delivery (33). Although enhanced stability of crystalline compounds has been well documented for small molecules, little is known about the stability of ordered self-assembly proteins. Unlike traditional small molecules, proteins possess higher order structures, which are required for biological activity. Whereas instability of small molecules involves only chemical pathways of degradation, instability of proteins includes both chemical degradation and physical denaturation. The latter relates to the loss of the bioactivity and more importance for clinical application. The observation in this work is likely a result of the crystalline environment providing an inert and rigid envitonment for the molecule that dose not readily allow the motion needed for reactions to occur. The inter- and intra-molecular interactions in the crystal lattice led to reduction in mobility that involving a significant fraction of the functional groups.

Further model building and comparison with the native rhIFN structure will hopefully elucidate how this delayed action is brought about through finding and describing the possible binding site and mode (seen in Fig. 10). Interferon-α belongs to type I interferons, which are helical cytokines with antiviral, immunomodulatory and proliferation regulatory activities. Structurally, they are all characterized by a five-helical topology (34). The crystal structure of rhIFN alpha-2b derived from Protein Data Bank shows that the proteins can form symmetry dimmers. The extensive dimmer interactions are mediated by a distorted tetrahedral coordination that is comprised by a zinc ion and glutamate (Glu41 and Glu42) located at the helix of each two-fold related molecule. On the opposite end of the dimerization interface, a potential salt bridge is formed by glutamate (Glu132) and Arginine (Arg33) and represented as surface mesh. In addition, residues along the dimer interface are majorly charged, which resulting in the dimerizing status highly dependent on the pH value and ionic strength of surroundings.

Compared with other essential trace metal elements, such as Fe, Cu, Co, Mg, *etc*., zinc usually possess particular advantageous features and hence favorable aspects in applications for medical use. Zinc is an efficient Lewis acid, making it a useful catalytic agent in hydroxylation and other enzymatic reactions. The metal also has a flexible coordination geometry, which allows proteins using it to rapidly shift conformations to perform biological reactions (35). It interacts with "a wide range of organic ligands" and has roles in the metabolism of RNA and DNA, signal transduction, gene expression and apoptosis regulation. Its low toxicity can be well explained by these features. In the human body, generally 2–3 g of zinc is present and about 15 mg per day is necessary for the maintenance of healthy condition (36). Therefore, zinc ions were employed preferentially in this work for chelation with rhIFN.

To relate rhIFN *in vitro* release kinetics from the aggregation to *in vivo* pharmacokinetic data, an *In Vitro/in Vivo* Correlation (IVIVC) analysis was performed to estimate *in vivo* pharmacokinetics behaviours from its *in vitro* dissolution performance. Among all the five levels of correlation, level A correlation is widely accepted by the regulatory agencies since which is the highest category of correlation and represents a point-to-point relationship between *in vitro* dissolution rate and *in vivo* absorption profile of the drug from the dosage form (37). The technique represents a major advance over the single-point approach due to utilizing all of the dissolution and plasma level data available to develop the correlations. Therefore, a change in manufacturing site, method of manufacture, raw material supplies and minor formulation modification can be justified without the need for additional *in vivo* studies. In this work, the *in vivo* percent of drug absorbed after s.c. administration at each time period was estimated by the Wagner−Nelson procedure with the pharmacokinetics parameters obtained (38). A visual inspection of the plots depicting the percentage of drug absorbed *versus* the amount of drug released *in vitro* shows a good correlation coefficient ($R^2 > 0.95$) and suggests a good correlation of the release profiles. The good IVIVC between the *in vitro* release (Dulbecco's phosphate-buffered saline, pH 7.4 at 37°C) and the cumulative fraction absorbed suggests that the proposed *in vitro* release method is well correlated to *in vivo* performance and may be used to further develop long-acting rhIFN formulations for the effective management of related disease.

CONCLUSION

In this paper, the self-assemblies of rhIFN with desirable yields were successfully prepared. The controllable release

profiles both *in vitro* and *in vivo* have been achieved by modulating the aggregated forms of rhIFN, yet the biological potency was remained enough to support the pharmacological activity. The findings make rhIFN self-assemblies in random amorphous or spherical crystal-like ordered forms, potential candidates for local sustained-release application of therapeutic proteins.

ACKNOWLEDGMENTS AND DISCLOSURES

The authors wish to thank the National Natural Science Foundation of China (No. 81072604 / 31170967) for financial support.

REFERENCES

1. Carter PJ. Introduction to current and future protein therapeutics: a protein engineering perspective. Exp Cell Res. 2011;317 (9):1261–9.
2. Szlachcic A, Zakrzewska M, Otlewski J. Longer action means better drug: tuning up protein therapeutics. Biotechnol Adv. 2011;29(4):436–41.
3. Fu K, Klibanov AM, Langer R. Protein stability in controlled-release systems. Nat Biotechnol. 2000;18(1):24–5.
4. Kozlowski A, Charles SA, Harris JM. Development of Pegylated interferons for the treatment of chronic hepatitis C. BioDrugs. 2001;15(7):419–29.
5. Dusheiko G. Side effects of alpha interferon in chronic hepatitis C. Hepatology. 1997;26(3 Suppl 1):112S–21.
6. Putney SD, Burke PA. Improving protein therapeutics with sustained-release formulations. Nat Biotechnol. 1998;16(2):153–7.
7. Zhang L, Schwendeman SP. Injectable biodegradable polymer depots for minimally invasive delivery of peptides and proteins. Adv Exp Med Biol. 2009;611:611–3.
8. Sinha VR, Trehan A. Biodegradable microspheres for protein delivery. J Control Release. 2003;90(3):261–80.
9. Weiner AL. Liposomes for protein delivery: selecting manufacture and development processes. ImmunoMethods. 1994;4(3):201–9.
10. Nelson DM, Ma Z, Leeson CE, Wagner WR. Extended and sequential delivery of protein from injectable thermoresponsive hydrogels. J Biomed Mater Res A. 2012;100(3):776–85.
11. Bailon P, Won CY. PEG-modified biopharmaceuticals. Expert Opin Drug Deliv. 2009;6(1):1–16.
12. Wang W, Nema S, Teagarden D. Protein aggregation–pathways and influencing factors. Int J Pharm. 2010;390(2):89–99.
13. Dobson CM. Principles of protein folding, misfolding and aggregation. Semin Cell Dev Biol. 2004;15(1):3–16.
14. Philo JS, Arakawa T. Mechanisms of protein aggregation. Curr Pharm Biotechnol. 2009;10(4):348–51.
15. Dunn MF. Zinc-ligand interactions modulate assembly and stability of the insulin hexamer – a review. Biometals. 2005;18(4):295–303.
16. Ding F, Dokholyan NV. Dynamical roles of metal ions and the disulfide bond in Cu, Zn superoxide dismutase folding and aggregation. Proc Natl Acad Sci U S A. 2008;105(50):19696–701.
17. Mattiasson B, Kumar A, Ivanov AE, Galaev IY. Metal-chelate affinity precipitation of proteins using responsive polymers. Nat Protoc. 2007;2(1):213–20.
18. Ochi T, Bolanos-Garcia VM, Stojanoff V, Moreno A. Perspectives on protein crystallisation. Prog Biophys Mol Biol. 2009;101(1–3):56–63.
19. Gietz U, Arvinte T, Häner M, Aebi U, Merkle HP. Formulation of sustained release aqueous Zn-hirudin suspensions. Eur J Pharm Sci. 2000;11(1):33–41.
20. Govardhan C, Khalaf N, Jung CW, Simeone B, Higbie A, Qu S, Chemmalil L, Pechenov S, Basu SK, Margolin AL. Novel long-acting crystal formulation of human growth hormone. Pharm Res. 2005;22(9):1461–70.
21. Jen A, Merkle HP. Diamonds in the rough: protein crystals from a formulation perspective. Pharm Res. 2001;18(11):1483–8.
22. Haris PI, Chapman D. Analysis of polypeptide and protein structures using Fourier transform infrared spectroscopy. Methods Mol Biol. 1994;22:183–202.
23. Venyaminov YS, Yang JT. Determination of protein secondary structure. In: Fasman GD, editor. Ircular dichroism and the conforma tional analysis of biomolecules. New York: Plenum; 1996. p. 69–107.
24. Yun J, Choi H. Micellar colorimetric determination of iron, cobalt, nickel and copper using 1-nitroso-2-naphthol. Talanta. 2000;52 (5):893–902.
25. Hallas-Moller K, Petersen K, Schlichtkrull J. Crystalline and amorphous insulin-zinc compounds with prolonged action. Science. 1952;116(3015):394–8.
26. Basu SK, Govardhan CP, Jung CW, Margolin AL. Protein crystals for the delivery of biopharmaceuticals. Expert Opin Biol Ther. 2004;4(3):301–17.
27. Gránásy L, Pusztai T, Börzsönyi T, Warren JA, Douglas JF. A general mechanism of polycrystalline growth. Nat Mater. 2004;3 (9):645–50.
28. Bassett DC. Polymer spherulites: a modern assessment. J Macromol Sci Phys. 2003;42(2):227–56.
29. Rogers SS, Krebs MR, Bromley EH, van der Linden E, Donald AM. Optical microscopy of growing insulin amyloid spherulites on surfaces *in vitro*. Biophys J. 2006;90(3):1043–54.
30. Wiencek JM. New strategies for protein crystal growth. Annu Rev Biomed Eng. 1999;1:505–34.
31. Chayen NE, Saridakis E. Protein crystallization: from purified protein to diffraction-quality crystal. Nat Methods. 2008;5:147–53.
32. Carter WA. Interferon: evidence for subunit structure. Proc Natl Acad Sci USA. 1970;67(2):620–8.
33. Frokjaer S, Otzen DE. Protein drug stability: a formulation challenge. Nat Rev Drug Discov. 2005;4:298–306.
34. Radhakrishnan R, Walter LJ, Hruza A, Reichert P, Trotta PP, Nagabhushan TL, Walter MR. Zinc mediated dimer of human interferon-alpha 2b revealed by X-ray crystallography. Structure. 1996;4(12):1453–63.
35. Favier A. Is zinc a cellular mediator in the regulation of apoptosis? metal ions in biology and medicine. In: Colley P, Bratter P, de Bratter VN, Khassanova L, Etienne JC, editors. Metal ions in biology and medicine volume 5. Paris: John Libbey Eurotex; 1998. p. 164–8.
36. Walsh CT, Sandstead HH, Prasad AS, Newberne PM, Fraker PJ. Zinc: health effects and research priorities for the 1990s. Environ Health Perspect. 1994;102 Suppl 2:5–46.
37. Amidon GL, Lennernäs H, Shah VP, Crison JR. A theoretical basis for a biopharmaceutic drug classification: the correlation of *in vitro* drug product dissolution and *in vivo* bioavailability. Pharm Res. 1995;12(3):413–20.
38. Emami J. *In vitro - in vivo* correlation: from theory to applications. J Pharm Pharm Sci. 2006;9(2):169–89.